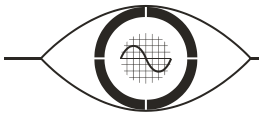

Lehrstuhl für Bildverarbeitung
Institute of Imaging & Computer Vision

Multispectral Image Acquisition with Flash Light Sources

Johannes Brauers and Stephan Helling and Til Aach
Institute of Imaging and Computer Vision
RWTH Aachen University, 52056 Aachen, Germany
tel: +49 241 80 27860, fax: +49 241 80 22200
web: www.lfb.rwth-aachen.de

in: Journal of Imaging Science and Technology. See also BIBTEX entry below.

BIBTEX:

```
@article{BRA09a,
author     = {Johannes Brauers and Stephan Helling and Til Aach},
title      = {Multispectral Image Acquisition with Flash Light Sources},
journal    = {Journal of Imaging Science and Technology},
publisher  = {IS\&T},
volume     = {},
number     = {},
year       = {2009},
pages      = {in press}}
```


document created on: November 28, 2008
created from file: paper.tex
cover page automatically created with CoverPage.sty
(available at your favourite CTAN mirror)

RWTH AACHEN
RHEINISCH-WESTFÄLISCHE TECHNISCHE HOCHSCHULE AACHEN

Multispectral Image Acquisition with Flash Light Sources

Johannes Brauers *
Institute of Imaging & Computer Vision, RWTH Aachen University

Stephan Helling †
Color and Image Processing Research Group, RWTH Aachen University

Til Aach ‡
Institute of Imaging & Computer Vision, RWTH Aachen University

November 28, 2008

*Templergraben 55, D-52056 Aachen, Germany, Tel.: 0049 241 8027866, Fax: 0049 241 8022200, Email: Johannes.Brauers@lfb.rwth-aachen.de

†Templergraben 55, D-52056 Aachen, Germany, Tel.: 0049 241 8027718, Alt. tel.: 0049 241 55958816, Email: helling@ite.rwth-aachen.de

‡Templergraben 55, D-52056 Aachen, Germany, Tel.: 0049 241 8027860, Fax: 0049 241 8022200, Email: Til.Aach@lfb.rwth-aachen.de

Abstract

We set up a multispectral image acquisition system using a flash light source and a camera featuring optical bandpass filters. The filters are mounted on a computer-controlled filter wheel between the lens and a grayscale sensor. For each filter wheel position, we fire the flash once within the exposure interval and acquire a grayscale image. Finally, all grayscale images are combined into a multispectral image. The use of narrowband filters to divide the electromagnetic spectrum into several passbands drastically reduces the available light at the sensor. In case of continuous light sources, this requires powerful lamps producing a lot of heat and long exposure times. In contrast, a flashgun emits its energy in a very short time interval, allowing for short exposure times and low heat production. Our detailed colorimetric analysis comparing the color accuracy obtainable with our flashgun and a halogen bulb shows that our acquisition system is well suited for multispectral image acquisition. We computed a mean color error of 1.75 CIEDE00 using the flashgun. Furthermore, we discuss several practical aspects arising from the use of flash light sources, namely the spectrum, repeat accuracy, illumination uniformity, synchronization and calibration of the system. To compensate for intensity variations of the flash, we propose two calibration methods and compare their performance.

Keywords: multispectral imaging, flash light source, intensity calibration, color accuracy.

1 Introduction

Multispectral cameras offer a lot of advantages over conventional three-channel cameras due to the fact that the spectral information of each pixel of the recorded scene is made available to the user.[1] This spectral information can be used to compute the tristimulus values of the scene under any given illuminant and for arbitrary observers with very high color accuracy. Today, a high number of multispectral imaging devices are studied or already in use worldwide.[2–9] Typical applications are archiving of paintings,[7,10,11] textile industry,[12–15] printing industry,[16] high dynamic range imaging (HDR),[17,18] HDTV video,[19] medicine,[20] and many others.[21–25] Conventional RGB photography on the other hand allows for the production of pleasant images, but is not capable of producing images with high color accuracy due to the violation of the Luther rule[26] and the lack of spectral information.[27–29] Nevertheless, researchers addressed the problem of color correction.[30,31]

In the case of multispectral cameras, the spectral information is acquired by utilizing an increased number of spectral passbands compared to conventional photography. For each of these channels, a grayscale image we call *frame* is taken. There are a number of well known reconstruction and estimation algorithms available today that compute the spectral information and/or tristimulus values from these frames.[32–37] While the number of filters is principally not limited, there is a commercial need to reduce their number to the absolutely necessary. Due to the relative smoothness of reflectance spectra, only a quite small number of filters is in fact necessary to allow for a highly accurate spectral estimation.[38,39]

The seven-band mobile multispectral camera that we use for our experiments has been developed by the Color Science and Color Image Processing Research Group at the RWTH Aachen University in the recent years.[32] It is equipped with a filter wheel that houses seven narrow band interference filters whose spectral transmittance curves are arranged equidistantly in the visible part of the spectrum. The filter wheel is mounted inside the camera between lens and sensor and not in front of the light source. Furthermore, the dimensions of the camera are relatively small. For these reasons, the camera can to some extent be used as a mobile device with arbitrary light sources. In the laboratory, we usually use halogen light sources.

Due to the spectral narrowness of the optical filters, only a small portion of the electromagnetic energy reaches the imaging sensor. Furthermore, short exposure times are desirable, because they minimize the overall acquisition time. One way to maximize the energy impinging on the sensor and at the same time minimize the exposure times is to use high power lamps that, unfortunately, produce a lot of heat. The second way which is focused on in this paper is the use of a flash gun as light source. Only very little heat is generated by such devices, and the light energy is emitted during a very short time interval. On the one hand, this requires synchronization between camera and flash gun, but on the other hand, the exposure times can be reduced drastically.

In this paper, some results on multispectral imaging with flash light sources we performed in a laboratory environment are presented. There are a number of practical and theoretical issues arising from using flash light sources for multispectral imaging, such as reproducibility of the amount of emitted light and reproducibility of the shape of the spectrum. Furthermore, the shape of the spectral power distribution of the emitted light must be dealt with. Unlike smooth spectra of thermal light sources, spectra of flash lights exhibit strong peaks. In this work we investigate the effect of these peaks on the multispectral image, i.e., we compare the quality of the spectral estimation for light sources with both peaky and smooth spectral distributions in both experiment and simulation.

This paper is organized as follows: In the next section, we outline a theoretical multispectral

imaging framework that incorporates intensity variations of the flashgun. We provide two methods to compensate for the variations. The third section describes the setup of our measurement stand and the processing steps we carry out to derive a multispectral image. Measurements of the flashgun and detailed colorimetric measurements are then presented in the forth section before we finish with the conclusions.

2 Theory

When using a continuous light source, its intensity can normally be considered as constant over time– at least after a warm-up phase. As will be shown later in this paper, this does not hold for our flash light source. In the following, we derive a spectral imaging model and estimation method taking the brightness variations into account. We start with the spectral imaging model describing the transformation of a reflectance spectrum to a sensor response. After that, the spectral estimation method utilizing a diagonal adaptation matrix $\mathbf{D}$ accounting for the brightness variations is shown. Finally, the computation of $\mathbf{D}$ itself is described in the last part of this section.

2.1 Spectral Imaging Model

We use sampled spectra in our model, since typical measured reflectance spectra are smooth. In our case, we use $N = 61$ spectral samples, thus covering a wavelength range from $\lambda_1 = 400\,\mathrm{nm}$ to $\lambda_N = 700\,\mathrm{nm}$ in steps of 5 nm. Furthermore, we omit the spatial dependencies in our equations, e.g., we write $\boldsymbol{\beta}$ instead of $\boldsymbol{\beta}_{x,y}$ for a reflectance spectrum without loss of generality.

In the noiseless case, the mapping of spectral sample values $\boldsymbol{\beta}$ to a sensor response $\mathbf{q}$ is described by

$$\mathbf{q} = f\left(\mathbf{KHS}\boldsymbol{\beta}\right) = f\left(\boldsymbol{Q}\right), \tag{1}$$

where the bold symbols denote vectors or matrices defined by

$$\begin{aligned}
\mathbf{q} &= \left(q_1 \dots q_I\right)^T && (I \times 1)\\
\boldsymbol{Q} &= \left(Q_1 \dots Q_I\right)^T && (I \times 1)\\
\mathbf{K} &= \mathrm{diag}\left(K_1 \dots K_I\right) && (I \times I)\\
\mathbf{H}_i &= \left(H_i(\lambda_1) \dots H_i(\lambda_N)\right)^T && (N \times 1)\\
\mathbf{H} &= \left(\mathbf{H}_1 \dots \mathbf{H}_I\right)^T && (I \times N)\\
\mathbf{S} &= \mathrm{diag}\left(S(\lambda_1) \dots S(\lambda_N)\right) && (N \times N)\\
\boldsymbol{\beta} &= \left(\beta(\lambda_1) \dots \beta(\lambda_N)\right)^T && (N \times 1)\,.
\end{aligned}$$

The operator $\mathrm{diag}(\cdot)$ constructs a diagonal matrix from a vector, $()^T$ denotes a transpose operation and I is the number of bandpass filters of the multispectral camera. The diagonal matrix $\mathbf{S}$ represents the light source. The effective spectral sensitivity matrix $\mathbf{H}$, joining the camera sensor sensitivity and bandpass filter transmission curves, transforms N spectral values to an I-dimensional sensor response. The continuous representation of $\mathbf{H}$ is plotted in Fig. 4. The diagonal channel scaling matrix $\mathbf{K}$ takes a factor for each spectral bandpass channel into account. It depends on the aperture and sensor

of the camera, as well as the exposure time for continuous light sources or flash intensity for flash light sources. The camera transfer function (CTF) $f()$, also known as *opto-electronic conversion function*, characterizes nonlinearities between the irradiance impinging on the sensor and the quantized sensor response; this includes the black level of the camera. If the black level is subtracted from the grayscale image in advance, the CTF is modified accordingly to prevent a duplicate subtraction of the black point. Since the linearization $\boldsymbol{Q} = f^{-1}(\mathbf{q})$ can be done in advance and the further postprocessing can be described without an explicit inclusion of it, we rewrite Eq. (1) to derive the linearized sensor response

$$\boldsymbol{Q} = \mathbf{KHS}\boldsymbol{\beta}. \tag{2}$$

2.2 Spectral Estimation

To estimate the diagonal channel scaling matrix $\mathbf{K}$ in Eq. (2), we perform a *multispectral white balance*: We use a white reference target with a known reflectance spectrum $\boldsymbol{\beta}_{\text{ref}}$, capture the reference sensor responses $\boldsymbol{Q}_{\text{ref}}$ for this specific target and compute the matrix

$$\mathbf{K}_{\text{ref}} = \operatorname{diag}\left(\boldsymbol{Q}_{\text{ref}} \div (\mathbf{HS}\boldsymbol{\beta}_{\text{ref}})\right) \tag{3}$$

by inversion of Eq. (2). The inversion is derived by the division of the $(I \times 1)$ vector $\boldsymbol{Q}$ by the term $\mathbf{HS}\boldsymbol{\beta}$, which is also an $(I \times 1)$ vector. The operator $\div$ denotes an element-wise division and $\operatorname{diag}(\cdot)$ forms the diagonal matrix $\mathbf{K}_{\text{ref}}$. Usually, the multispectral white balance is performed once before the measurements and the calculated reference channel scaling matrix $\mathbf{K}_{\text{ref}}$ is used for normalization.

When using flash light sources, the intensity of the flashgun may vary with each exposure and invalidate the white balance calibration. For example, the reference sensor responses $\boldsymbol{Q}_{\text{ref}}$ taken for the white reference target may change for a second reference measurement. We incorporate the fluctuations by relating the reference channel scaling matrix $\mathbf{K}_{\text{ref}}$ to the actual channel scaling matrix $\mathbf{K}$ using

$$\mathbf{K} = \mathbf{D}\mathbf{K}_{\text{ref}}\,, \tag{4}$$

where $\mathbf{D}$ is an $(I \times I)$ diagonal matrix. If the light source stays constant over time, which is the case for, e.g., a heat light source after its warm-up phase, $\mathbf{D}$ is an identity matrix. Using Eq. (4), we insert Eq. (3) into Eq. (2) and derive

$$\begin{aligned} \boldsymbol{Q} &= \mathbf{D}\operatorname{diag}\left(\boldsymbol{Q}_{\text{ref}} \div (\mathbf{HS}\boldsymbol{\beta}_{\text{ref}})\right)\mathbf{HS}\boldsymbol{\beta} \\ &= \mathbf{D}\operatorname{diag}\left(\boldsymbol{Q}_{\text{ref}}\right)\operatorname{diag}\left(\mathbf{HS}\boldsymbol{\beta}_{\text{ref}}\right)^{-1}\mathbf{HS}\boldsymbol{\beta} \end{aligned} \tag{5}$$

and by further simplification

$$\mathbf{D}^{-1}\left(\boldsymbol{Q} \div \boldsymbol{Q}_{\text{ref}}\right) \circ (\mathbf{HS}\boldsymbol{\beta}_{\text{ref}}) = \mathbf{HS}\boldsymbol{\beta}\,, \tag{6}$$

where the operator "$\circ$" denotes an element-wise multiplication. The simplification is derived by utilizing the diagonal matrices in Eq. (5). The division of $\boldsymbol{Q}$ by $\boldsymbol{Q}_{\text{ref}}$ can be interpreted as a multispectral white balance, where $\mathbf{D}$ is a correction term accounting for intensity changes of the light source between the acquisition of the white reference target and the color target.

The estimated reflectance $\hat{\boldsymbol{\beta}}$ can finally be computed from Eq. (6) by

$$\hat{\boldsymbol{\beta}} = \mathbf{H}_{\text{inv}}\mathbf{D}^{-1}\left(\boldsymbol{Q} \div \boldsymbol{Q}_{\text{ref}}\right) \circ \left(\mathbf{HS}\boldsymbol{\beta}_{\text{ref}}\right) , \tag{7}$$

using the Wiener inverse[40]

$$\mathbf{H}_{\text{inv}} = \mathbf{R}_{xx}\left(\mathbf{HS}\right)^{T}\left(\mathbf{HSR}_{xx}\left(\mathbf{HS}\right)^{T}\right)^{-1} . \tag{8}$$

The matrix

$$\mathbf{R}_{xx} = \begin{pmatrix} 1 & \rho & \rho^2 & \cdots & \rho^{N-1} \\ \rho & 1 & \rho & \cdots & \rho^{N-2} \\ \rho^2 & \rho & 1 & & \vdots \\ & \vdots & & \ddots & \rho \\ \rho^{N-1} & \rho^{N-2} & \cdots & \rho & 1 \end{pmatrix} \tag{9}$$

models the reflectance $\boldsymbol{\beta}$ as being smooth, i.e., neighboring values are assumed to be correlated by a factor ρ; a typical value for ρ is 0.98. By using the pseudoinverse without weighting, a strong oscillation of the solution might result.

2.3 Intensity Calibration Methods

To account for the varying intensity of the flashgun, we studied two options: Our *intrinsic* calibration utilizes a reference patch with known reflectance spectrum $\boldsymbol{\beta}_{\text{ref}}$ inside the scene to normalize the sensor response. The reference channel scaling matrix $\mathbf{K}_{\text{ref}}$ can then be estimated by Eq. (3). This approach provides a very reliable estimation of the image brightness since the reference patch is directly measured by the camera itself. However, in some applications it might not be feasible to place an additional target in the scene.

The *extrinsic* calibration relies on the measurements of an external measurement device in order to relate the calibration data taken with the white reference card to the acquired color image. More specifically, the external sensor allows us to estimate the diagonal matrix $\mathbf{D}$ in Eq. (4). We use a spectral photometer which measures the spectrum each time the flash is fired and derive a matrix $\mathbf{S} = (\mathbf{S}_1 \ldots \mathbf{S}_I)$, where each $\mathbf{S}_i$ is a vector $(N \times 1)$ with the spectrum of the light source. With external measurement values $\mathbf{S}_{\text{ref}}$ for the white reference target and $\mathbf{S}$ for the color image, we compute the adaptation matrix

$$\mathbf{D} = \frac{\operatorname{diag}\left(\mathbf{HS}\right)}{\operatorname{diag}\left(\mathbf{HS}_{\text{ref}}\right)} , \tag{10}$$

where $\mathbf{H}$ is the effective spectral sensitivity introduced in Eq. (1).

When the spectrum of the flashgun scales linearly, a simple light sensor is sufficient for the measurement. Eq. (10) then reduces to

$$\mathbf{D} = \frac{\operatorname{diag}\left(\mathbf{v}\right)}{\operatorname{diag}\left(\mathbf{v}_{\text{ref}}\right)} , \tag{11}$$

where $\mathbf{v}$ $(I \times 1)$ is the light sensor response for the color image and $\mathbf{v}_{\text{ref}}$ is the one for the white reference image.

3 Practical Experiment

3.1 Setup and Acquisition

For flash image acquisition we use the setup depicted in Fig. 1, which basically represents a 45°/0° geometry: our multispectral camera is mounted perpendicular to the object plane, while the flashgun is placed at a 45° angle with respect to the sample normal. We directly measure the intensity of the flashgun with an additional light sensor in front of the flashgun; in our case, we use a GretagMacbeth EyeOne Pro spectral photometer. Other sensors could also be used.

Our multispectral camera features the ICX285 sensor with a resolution of 1280 × 960 pixel and a pixel cell size of 6.25 μm × 6.25 μm. The computer-controlled bandpass filter wheel exhibits seven filter positions, all of which are equipped with optical bandpass filters in the range between 400 nm and 700 nm, each with 40 nm bandwidth. The filter wheel is positioned between the grayscale sensor and the Nikkor AF-S DX 18-70mm lens. To achieve well-exposed images, we fired the flash at the intensity settings given in Tab. 2.

We use a studio flashgun "Star Light 250" from "Richter Studiogeräte GmbH", [1] which features a flash tube and an additional halogen bulb. Since both light sources are positioned very close to each other, their light distributions are supposed to be nearly identical. Thus, the halogen light source is used to setup the positioning of the flashgun. While acquiring the images with the flashgun, the halogen lamp was switched off. In turn, the flashgun was deactivated for the acquisition of images with the built-in halogen lamp. The maximum flash capacity of the device is 244 Ws and can be reduced by a potentiometer. In the following, we refer capacity specifications to the full exposure, e.g., we write 25% flash exposure for approximately 61 Ws flash capacity.

Fig. 3 shows a timing diagram for both flash and continuous light source imaging. For each spectral passband, the appropriate optical filter is brought into the optical path with the computer-controlled filter wheel. In the case of flashgun illumination, both camera and external light sensor (see Fig. 1) are then triggered. The flash is fired with the appropriate intensity within the windows of the exposure time of both devices. It is important that the flash exposure does not precede or exceed any of the other two devices' exposure times. These steps are repeated for each one of the seven optical filters, resulting in seven grayscale images we call spectral *frames*, where each *frame* represents the image information for one spectral passband. The camera exposure time has hardly any influence in case of flash light imaging, since the interval, where the flash emits its energy is very short. Of course, any illumination other than the flashgun should be suppressed during the acquisition; this particularly holds for long exposure times. When using continuous light sources for a comparative analysis, the exposure time of the camera controls the brightness of the image (Fig. 3b). In this case, we assumed the halogen light source to be constant over time and omitted the measurements with the spectral photometer.

We capture a black and white reference image to compensate for various camera- and illumination-specific irregularities as shown in the following section. The black reference image is taken with the lens cap attached to the lens. It enables us to compensate for the black point of the camera. For the acquisition of the white reference, we acquire a homogeneous white plate and determine the shading of the image to compensate for spatial inhomogeneities of the illumination. Additionally, the white plate serves as a spectral white reference to perform a multispectral white balance, i.e., we relate the sensor response of the scene to the sensor response of the white plate.

[1] Richter Studiogeräte GmbH, Am Riedweg 30, D-88682 Salem-Neufrach, Germany, `www.richterstudio.de`

Unlike the constant intensity of a continuous light source after its warm-up phase, the intensity of our flashgun varies for consecutive exposures as our experiments show below. This means that every frame, i.e., every grayscale image in the corresponding spectral passband, is possibly exposed with a different illumination intensity. Our experiments showed, that ignoring the varying intensity would lead to large color errors when combining the passbands to a color image. Therefore, we perform a calibration by measuring the flash intensity parallel to the camera exposure with a spectral photometer. Unlike the camera, our external sensor measures the light source directly and does not depend on the content of the scene. The measured intensities are used to correct each image by a factor.

3.2 Image Processing Pipeline

Fig. 5 shows an overview diagram of the postprocessing steps we apply to the frame data. The black and white reference image and the spectral frames are the input data of our processing chain. The black reference image is a single grayscale image, whereas the other ones are seven grayscale *frames* representing the seven spectral passbands. The black reference is subtracted from both the white reference and the spectral frames to compensate for the (spatially varying) black point. To account for nonlinearities, we linearize the sensor responses with the inverse CTF as shown above; we determine the CTF using our measurement stand.[18] Since the black point has been subtracted in advance, the CTF is adapted to exclude the black point.

We perform a shading correction to account for a spatially inhomogeneous illumination of the scene: To prepare the correction, the sensor response of the linearized white reference is divided by the linearized sensor response of a certain area of the image, as indicated by the rectangle in the image "white reference" of Fig. 5. Furthermore, the white reference is filtered with a lowpass kernel in order to remove small speckles and reduce noise.

We developed two methods for the compensation of intensity variations of the flashgun: The *intrinsic* calibration normalizes the image frame data using the linearized pixel values of a white reference patch in the spectral frame data. Since the white reference patch is also illuminated by the flash light, it allows for a direct measurement of the flash intensity. The normalization process is indicated in Fig. 5 with a small centered rectangle in the image "spectral frames" and a round box with a division operator "÷". Our *extrinsic* calibration method utilizes a white reference patch acquired from the white reference target. Since the flash intensities may vary between the acquisition of the white reference target and the color target, we compute a "scaling" factor to relate both target images using the external sensor. The adaptation procedure is described in detail in the second section of this paper. Both methods result in frame data containing solely the value *one* for pixels corresponding to the white reference patch. Since the spectrum of the white reference target typically does not exhibit a perfectly flat spectral distribution, e.g., in our case, it has a higher absorption in the blue part of the visible spectrum, the sensor responses have to be multiplied with the computed response of the white reference. To compensate for the (slightly) inhomogeneous illumination of the test target, we furthermore divide the color image by the lowpass-filtered white reference image.

The different thicknesses and refraction indices of the optical bandpass filters in our camera, as well as the possibly non-coplanar alignment of the filters in the filter wheel cause a space-dependent geometric distortion of the seven spectral frames. If the spectral frames are directly combined into a color image, large rainbow-like color fringes would be induced since the spectral color separations are not aligned. We use our compensation algorithm[41,42] to automatically correct the effects of the

optical aberrations. Finally, we estimate the spectrum for each image pixel, as shown before. A transformation to color spaces for visualization (monitor color space, sRGB) or measurement of color differences (L*a*b*) can then be performed.

4 Results

4.1 Flashgun Measurements

When using a flash light source, the brightness level of the image is controlled by the flash intensity rather than the exposure time of the camera. Therefore, we investigated the reproducibility of the flash spectrum at varying intensities. Our measurement device, a Dr. Gröbel[2] spectral photometer, has a spectral resolution of 0.6 nm and measures the spectral power distribution (SPD) from 200 nm to 800 nm. We fired the flash at varying intensities, in each case within the integration time of the photometer. To be able to compare the spectra, we normalized the SPDs by dividing them by their luminance value Y in the XYZ color space. In Fig. 6, we plotted the spectra at the lowest and highest intensity settings of the flash since their correlated color temperature (CCT)[43] differs the most (see below). Additionally, we computed the variance of all normalized flash spectra for each wavelength. Comparing the spectra for full and 6.25% exposure, we find that the spectrum for the full exposure shows an increased emission in the lower wavelength range and a decreased emission in the higher wavelength range. Considering the variance, we deduce that the spectra vary to a higher percentage at peak positions.

We also compared the tristimulus values using the CIE 1931 observer and the CCT for the flash spectra (see Tab. 1). The maximum deviation from the mean XYZ value is 0.65% for the X coordinate and 4.03% for the Z coordinate. The CCT spans a range of approximately 500 K, from 5740 K for the 6.25% exposure and 6238 K for the full flash exposure. Including all intensity settings, we computed a maximum color error of 4.24 ΔE_{00} units by transformation of the light source SPD to L*a*b* values. In our experiments, we use a smaller range of power settings, i.e., we approximately use a 25% to 100% exposure. This reduces the color error to 2.56 ΔE_{00}. Additionally, we perform the spectral calibration with the same power settings used for the final acquisition of the color image, reducing the effects of the color temperature shift.

Our extrinsic calibration method normalizes the image brightness utilizing the measurements of the external sensor. Since a linear relation between the values of both sensors is essential, we carried out simultaneous measurements of the flash intensity with the camera and the spectral photometer as shown in Fig. 7 to verify our approach. We performed the measurements using a constant power setting of our flashgun (25% exposure), selected the 550 nm optical bandpass filter in our multispectral camera and acquired an image of the white reference target. The sensor response was compensated for the black point and nonlinearities using the inverse CTF, and the spectra from the spectral photometer were transformed to luminance values using the CIE 1931 observer. By evaluating 21 images, we estimated a pulse-to-pulse variability of 5%, i.e., the 8-bit gray level values range from 138 to 145. The intensity variations confirmed the necessity of an external sensor for intensity calibration. To evaluate the deviation between both measurement devices, we computed a line of best fit shown in Fig. 7. We found a mean calibration error of 0.23 gray values corresponding to 0.89‰in terms of an

[2]Dr. Gröbel UV-Elektronik GmbH, Goethestraße 17, D-76275 Ettlingen, Germany, `http://www.uv-groebel.de/`

8 bit sensor. This justifies the use of an external sensor as an appropriate calibration device for our application.

We also investigated the illumination uniformity for consecutively acquired images. Therefore, the linearized images that were used above to measure the relation between both measurement devices were normalized by their global brightness. Additionally, a lowpass filtering with a 40×40 Gaussian kernel ($\sigma = 10$) was performed to reduce noise. The image in Fig. 8 was then derived by computing the variance for each image position over all exposures. Image areas with bright gray values denote a small variation, whereas areas with dark gray values correspond to larger variations. The sample values in the image denote variance values. Although there is a small variation of the illumination uniformity in the bottom right corner, the effects are negligible.

4.2 Colorimetric Measurements

Since the studio flash offers both a flash tube and a halogen light source with 150 W, we performed the flash and halogen experiments using the same apparatus and a fixed setup described in the third section. Doing so, both light sources are comparable regarding their light distribution in the target plane since they are positioned very close to each other. We used four test charts for our experiments, a GretagMacbeth ColorChecker with 24 color patches, a ColorChecker DC with 237 patches, a ColorChecker SG with 140 patches and a laboratory sample of the TE 221 chart with 283 color patches. The spectral reflectances of all chart patches have been measured using a spectral photometer (GretagMacbeth EyeOne Pro). We acquired and postprocessed the images using the procedure described in the previous section. The spectral values of each color patch were averaged out by computing the mean value over an area inside the color patch. We then computed both mean and maximum ΔE_{00} color errors using the illuminant D50. Most of the maximum errors are caused by glossy patches and stray light effects on very dark patches.

Our experimental results for different test charts and both light sources are denoted in Tab. 3, showing the mean and maximum color errors. The *intrinsic* calibration utilizes a patch in the test chart itself to adapt to the varying flash intensity. Our second calibration method, the *extrinsic* calibration, uses the measurements with the external sensor to relate the white reference vector taken from the white reference target to the acquired test chart. In other words, the intensity variations of the flashgun are taken into account for the multispectral white balance. For the results in the column "flash, omitted extr.", we omitted the adaptation by setting the factor $\mathbf{D}$ in Eq. (4) to the identity matrix. In doing so, we implicitly assumed a constant flash intensity. In this case, the estimation results are very poor. This highlights the requirement of an external sensor for calibration.

For all test charts, the color accuracy achieved by the flashgun with intrinsic calibration is comparable to the results obtained by the halogen bulb; the mean color errors are 1.75 ΔE_{00} and 1.77 ΔE_{00}, respectively. This justifies the use of a flashgun for accurate color image acquisition in a controlled laboratory environment. The extrinsic calibration produces almost the same results as the intrinsic one (mean color error: 1.78 ΔE_{00}). We also investigated different weightings to convert the spectrum measured by the spectral photometer into scalar adaptation factors: Using Eq. (10), we weighted the spectrum with the effective spectral sensitivities given in Fig. 4. On the other hand, Eq. (11) describes the transformation of the spectrum to a luminance value Y utilizing the CIE 1931 observer and does not incorporate a wavelength dependency. Here, the spectral measurement is reduced to a light sensor measurement. The results of both weighting methods were practically identical and show that a linear light sensor is sufficient to compensate for the intensity variations. When we omit the extrinsic cal-

ibration (column "flash, omitted extr."), the color errors increase drastically in cases where the flash intensity varies a lot between the acquisition of the white reference target and the test chart. This applies for the ColorChecker with 24 patches and the ColorChecker SG. The mean color error increases to 2.84 ΔE_{00}.

To give a more detailed view, we provide a color error report for each color patch in Fig. 9 and Fig. 11 and provide the corresponding histograms in Fig. 10 and Fig. 12, respectively. Due to stray light in our camera, some of the dark patches exhibit an increased color error. As noted before, some glossy patches, e.g., in the column 'S' from ColorChecker DC, also cause rather large color errors. Independent of these camera specific issues, the color accuracy for the acquisition of our test charts could be improved by using a training data set instead of a fixed correlation factor ρ for our spectral estimation matrix in Eq. (8). But by doing so, we would adapt to the specific data set and lose generality.

We performed a simulation with the spectral data of the test charts we used for the experiment as well as with the Vrhel data set.[44] Besides the simulation using the spectra of the flashgun and the halogen light source, we also used the illuminants 'A', 'D50' and 'D65'. The results are denoted in Tab. 4. The illuminants A, D50 and D65 are arranged on the left hand side of the table, whereas the light sources used for our experiment are on the right hand side. We decided to use the measured spectrum of the flashgun at the 25% exposure. The results show an almost equal color error of 0.6 ΔE_{00} for the illuminants A, D50 and D65 and our halogen light source. Our flash light source has a slightly worse performance of 0.73 ΔE_{00}, but still offers a high color accuracy for the simulated seven spectral channels.

5 Conclusions

We have extended our multispectral image acquisition system using a flash light source. The measurements for our flashgun have shown a pulse-to-pulse variability of 5%; we therefore developed two compensation methods for the varying brightness of the acquired images: The *intrinsic* calibration utilizes a patch in the acquired image itself to measure the actual brightness and correct the image data accordingly. Our flashgun acquisition experiments with several test charts resulted in a color error of only 1.75 ΔE_{00}, which is almost identical to the color error produced by a comparative analysis with a halogen bulb (1.77 ΔE_{00}). Our *extrinsic* calibration method uses the measurements of an external sensor to account for the intensity changes. We computed the mean calibration error for the external sensor to only 0.23 gray values (8 bit range). This justifies the use of an external sensor and is also confirmed by the colorimetric measurements, which result in a similar color accuracy (1.78 ΔE_{00}) than the intrinsic calibration method. A simulation with both experimental light sources as well as other illuminants also certifies a good performance of the flashgun.

6 Acknowledgments

The authors are grateful to Professor Bernhard Hill, RWTH Aachen University, for many helpful discussions.

References

[1] B. Hill, High quality color image reproduction: The multispectral solution, in *9th International Symposium on Color Science and Applications MCS-07*, pages 1–7, Taipei, Taiwan, 2007.

[2] B. Hill and F. W. Vorhagen, Multispectral image pick-up system, 1991, U.S.Pat. 5,319,472, German Patent P 41 19 489.6.

[3] J. Y. Hardeberg, F. J. Schmitt, and H. Brettel, Multispectral image capture using a tunable filter, in *Color Imaging: Device-Independent Color, Color Hardcopy, and Graphic Arts*, San Jose, CA, USA, 2000.

[4] F. Schmitt, H. Brettel, and J. Y. Hardeberg, *Multispectral Imaging Development at ENST*, Display and Imaging **8**, 261 (2000).

[5] B. Hill, Aspects of total multispectral image reproduction systems, in *2nd International Symposium on High Accurate Color Reproduction and Multispectral Imaging*, Chiba University, Japan, 2000.

[6] M. Rosen, F. Imai, X. Jiang, and N. Ohta, Spectral reproduction from scene to hardcopy I: Input and output, in *IS&T/SPIE Electronic Imaging*, San Jose, CA, USA, 2001.

[7] R. S. Berns, *The Science of Digitizing Paintings for Color-Accurate Image Archives: A Review*, Journal of Imaging Science and Technology **45**, 305 (2001).

[8] H. Haneishi, T. Iwanami, T. Honma, N. Tsumura, and Y. Miyake, *Goniospectral Imaging of Three-Dimensional Objects*, Journal of Imaging Science and Technology **45**, 451 (2001).

[9] J. Y. Hardeberg and J. Gerhardt, Towards spectral color reproduction, in *9th International Symposium on Color Science and Applications MCS-07*, Taipei, Taiwan, 2007.

[10] H. Liang, D. Saunders, J. Cupitt, and M. Benchouika, A new multi-spectral imaging system for examining paintings, in *Colour in Graphics, Imaging, and Vision (CGIV)*, pages 229–234, Aachen, Germany, 2004.

[11] V. Bochko, N. Tsumura, and Y. Miyake, *Spectral Color Imaging System for Estimating Spectral Reflectance of Paint*, Journal of Imaging Science and Technology **51**, 70 (2007).

[12] T. Keusen, *Multispectral Color System with an Encoding Format Compatible with the Conventional Tristimulus Model*, Journal of Imaging Science and Technology **40**, 510 (1996).

[13] D. Steen and D. Dupont, *Defining a Practical Method of Ascertaining Textile Color Acceptability*, Wiley's Color Research & Application **27**, 391 (2002).

[14] P. G. Herzog, Virtual fabrics or multispectral imaging in B2B, in *IS&Ts Proc. 1st European Conference on Color in Graphics, Imaging and Vision (CGIV)*, pages 580–584, Poitiers, France, 2002.

[15] P. G. Herzog and B. Hill, Multispectral imaging and its applications in the textile industry and related fields, in *PICS, Digital Photography Conference*, Rochester, NY, USA, 2003.

[16] S. Yamamoto, N. Tsumura, and T. Nakaguchi, *Development of a Multi-spectral Scanner using LED Array for Digital Color Proof*, Journal of Imaging Science and Technology **51**, 61 (2007).

[17] H. Haneishi, S. Miyahara, and A. Yoshida, *Image acquisition technique for high dynamic range scenes using a multiband camera*, Wiley's Color Research & Application **31**, 294 (2006).

[18] J. Brauers, N. Schulte, A. A. Bell, and T. Aach, Multispectral high dynamic range imaging, in *IS&T/SPIE Electronic Imaging*, San Jose, California, USA, 2008.

[19] K. Ohsawa et al., *Six Band HDTV Camera System for Spectrum-Based Color Reproduction*, Journal of Imaging Science and Technology **48**, 85 (2004).

[20] M. Nishibori, N. Tsumura, and Y. Miyake, *Why Multispectral Imaging in Medicine?*, Journal of Imaging Science and Technology **48**, 125 (2004).

[21] S. Tominaga, *Spectral Imaging by a Multispectral Camera*, Journal of Electronic Imaging **8**, 332 (1999).

[22] M. Hauta-Kasari, K. Miyazawa, S. Toyooka, and J. Parkkinen, *Spectral Vision System for Measuring Color Images*, Journal of the Optical Society of America **16**, 2352 (1999).

[23] R. Baribeau, *Application of Spectral Estimation Methods to the Design of a Multispectral 3D Camera*, Journal of Imaging Science and Technology **49**, 256 (2005).

[24] W. Wu, J. P. Allebach, and M. Analoui, *Imaging Colorimetry Using a Digital Camera*, Journal of Imaging Science and Technology **44**, 267 (2000).

[25] M. Vilaseca, M. de Lasarte, J. Pujol, M. Arjona, and F. H. Imai, Estimation of human iris spectral reflectance using a multi-spectral imaging system, in *Colour in Graphics, Imaging, and Vision (CGIV)*, pages 232–236, Leeds, Great Britain, 2006.

[26] R. Luther, *Aus dem Gebiet der Farbreizmetrik*, Zeitschrift für technische Physik **12**, 540 (1927).

[27] J. Orava, T. Jaaskelainen, and J. Parkkinen, *Color Errors of Digital Cameras*, Wiley's Color Research & Application **29**, 217 (2004).

[28] F. Martínez-Verdú, J. Pujol, and P. Capilla, *Characterization of a Digital Camera as an Absolute Tristimulus Colorimeter*, Journal of Imaging Science and Technology **47**, 279 (2003).

[29] F. König and P. Herzog, On the limitations of metameric imaging, in *Conference on Image Processing, Image Quality and Image Capture Systems*, pages 163–168, Savannah, Georgia, USA, 1999.

[30] G. D. Finlayson and P. M. Morovic, *Metamer Constrained Color Correction*, Journal of Imaging Science and Technology **44**, 295 (2000).

[31] P. Urban and R.-G. Grigat, *The Metamer Boundary Descriptor for Color Correction*, Journal of Imaging Science and Technology **49**, 418 (2005).

[32] S. Helling, E. Seidel, and W. Biehlig, Algorithms for spectral color stimulus reconstruction with a seven-channel multispectral camera, in *IS&Ts Proc. 2nd European Conference on Color in Graphics, Imaging and Vision (CGIV)*, pages 254–258, Aachen, Germany, 2004.

[33] F. H. Imai and R. S. Berns, Spectral estimation of artist oil paints using multi-filter trichromatic imaging, in *9th Congress of the International Colour Association*, Rochester, NY, USA, 2002.

[34] P. Stigell, K. Miyata, and M. Hauta-Kasari, Wiener estimation method in estimation of spectral reflectance from RGB image, in *7th International Conference on Pattern Recognition and Image Analysis*, St. Petersburg, Russia, 2004.

[35] A. Ribés, F. Schmitt, R. Pillay, and C. Lahanier, *Calibration and Spectral Reconstruction for CRISATEL: An Art Painting Multispectral Acquisition System*, Journal of Imaging Science and Technology **49**, 563 (2005).

[36] N. Shimano, Recovery of spectral reflectance of art paintings without prior knowledge of objects being imaged, in *10th Congress of the International Colour Association (AIC)*, Granada, Spain, 2005.

[37] P. Morovic and H. Haneishi, Estimating reflectances from multi-spectral video responses, in *14th Color Imaging Conference*, Scottsdale, Arizona, USA, 2006.

[38] J. Y. Hardeberg, *Filter Selection for Multispectral Color Image Acquisition*, Journal of Electronic Imaging **48**, 105 (2004).

[39] D. Connah, A. Alsam, and J. Y. Hardeberg, *Multispectral Imaging: How Many Sensors Do We need?*, Journal of Imaging Science and Technology **50**, 45 (2006).

[40] W. K. Pratt and C. E. Mancill, *Spectral estimation techniques for the spectral calibration of a color image scanner*, Applied Optics **15**, 73 (1976).

[41] J. Brauers, N. Schulte, and T. Aach, Modeling and compensation of geometric distortions of multispectral cameras with optical bandpass filter wheels, in *15th European Signal Processing Conference*, pages 1902–1906, Poznań, Poland, 2007.

[42] J. Brauers, N. Schulte, and T. Aach, *Multispectral Filter-Wheel Cameras: Geometric Distortion Model and Compensation Algorithms*, IEEE Transactions on Image Processing **17** (2008), to appear.

[43] G. Wyszecki and W.S.Stiles, *Color Science: Concepts and Methods, Quantitative Data and Formulae*, Wiley, 1982.

[44] M. J. Vrhel, R. Gershon, and L. S. Iwan, *Measurement and analysis of object reflectance spectra*, Color Research and Application **19**, 4 (1994).

Intensity setting	X	Y	Z	CCT
100%	0.9497	1.0000	1.0499	6238 K
50%	0.9532	1.0000	1.0180	6017 K
25%	0.9537	1.0000	1.0044	5933 K
12.5%	0.9550	1.0000	0.9930	5858 K
6.25%	0.9606	1.0000	0.9806	5740 K
mean	0.9544	1.0000	1.0092	5957 K

Table 1: Color coordinates of the flashgun in XYZ color space (normalized to $Y = 1$) and correlated color temperatures (CCT) for different flash intensity settings.

center wavelength	400 nm	450 nm	500 nm	550 nm	600 nm	650 nm	700 nm
intensity	100.00%	32.06%	26.65%	26.12%	31.01%	46.47%	85.04%

Table 2: Flash intensity for each spectral passband during the acquisition; the value "100%" denotes full exposure.

mean / max ΔE_{00}	flash intr.	flash extr.	flash, omitted extr.	halogen
ColorChecker	1.33 / 2.36	1.38 / 2.49	3.63 / 7.58	1.48 / 2.70
ColorChecker DC	1.58 / 7.24	1.72 / 6.91	1.73 / 6.94	1.71 / 6.34
ColorChecker SG	1.93 / 6.53	2.03 / 6.18	4.07 / 6.74	1.76 / 5.47
TE221	2.16 / 8.15	2.00 / 7.79	1.96 / 7.22	2.13 / 7.35
mean / maxi	1.75 / 8.15	1.78 / 7.79	2.84 / 7.58	1.77 / 7.35

Table 3: Experimental results comparing the performance (mean / max ΔE_{00}) of our flashgun with intrinsic, extrinsic and omitted extrinsic calibration (see text) against a halogen light source, calculated for illuminant D50 using the CIE 1931 observer.

mean / max ΔE_{00}	A	D50	D65	flash	halogen
Vrhel DuPont	0.67 / 1.79	0.66 / 1.74	0.67 / 1.74	0.72 / 2.24	0.71 / 1.92
Vrhel Munsell	0.54 / 1.73	0.54 / 1.64	0.54 / 1.63	0.66 / 2.37	0.58 / 1.86
Vrhel natObjects	0.46 / 3.38	0.44 / 3.12	0.44 / 2.96	0.73 / 3.64	0.48 / 3.65
ColorChecker	0.67 / 1.98	0.66 / 1.82	0.67 / 1.79	0.70 / 2.44	0.70 / 2.06
ColorChecker DC	0.61 / 2.02	0.60 / 1.91	0.61 / 1.88	0.78 / 2.59	0.66 / 2.15
ColorChecker SG	0.73 / 2.14	0.69 / 2.02	0.68 / 1.99	0.90 / 2.69	0.78 / 2.27
TE 221	0.54 / 2.87	0.55 / 2.81	0.56 / 2.81	0.61 / 2.87	0.57 / 2.89
mean / max	0.60 / 3.38	0.59 / 3.12	0.60 / 2.96	0.73 / 3.64	0.64 / 3.65

Table 4: Simulation results (mean / max ΔE_{00}) for various light sources and test charts, calculated for illuminant D50 using the CIE 1931 observer.

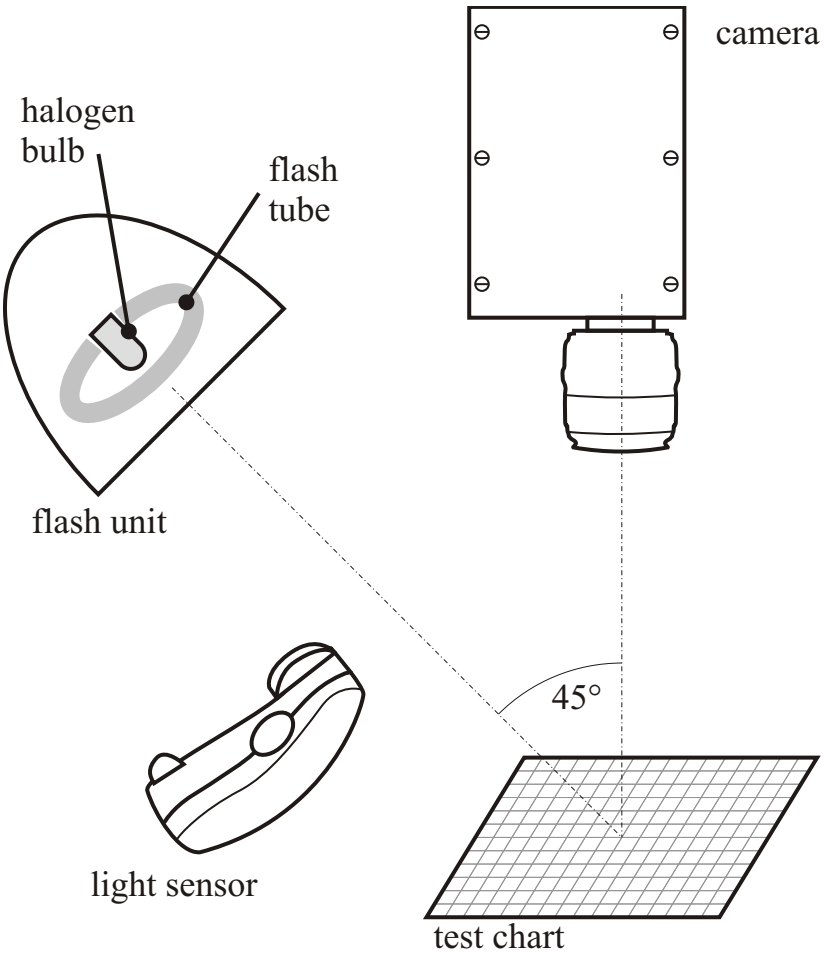

Figure 1: Our acquisition setup with the flash unit containing both flash and halogen light source.

Figure 2: Our multispectral camera and a sketch of its internal configuration.

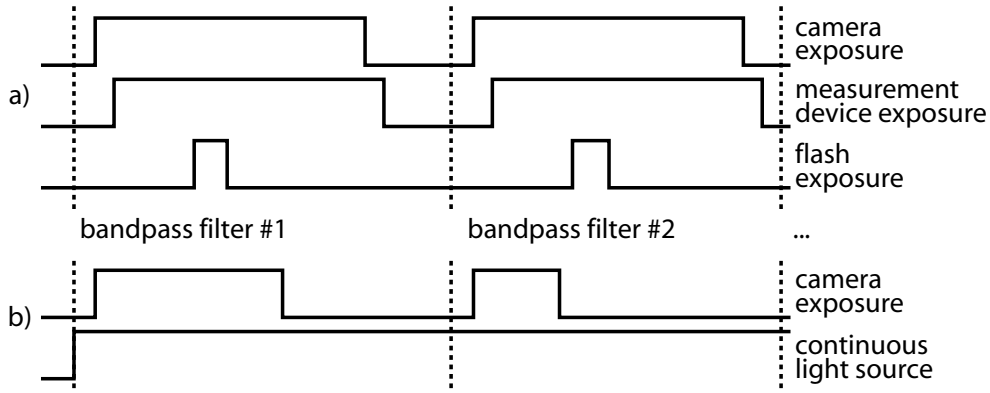

Figure 3: Timing diagram for a flash light source (a) and a continuous light source (b).

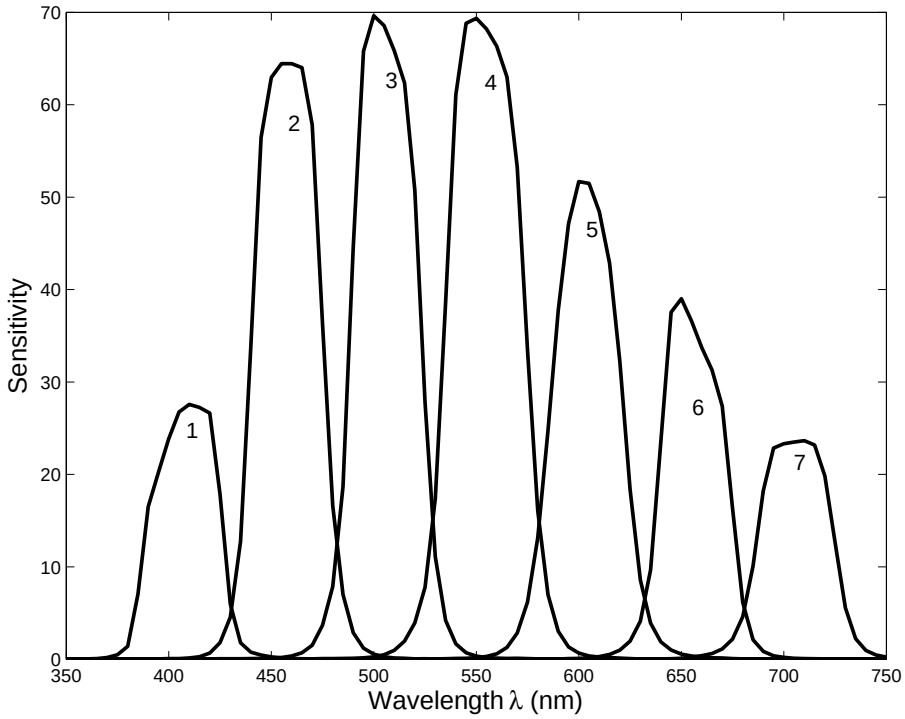

Figure 4: Continuous representation of the effective spectral sensitivity matrix $\mathbf{H}$ of our multispectral camera; each column corresponds to one plot.

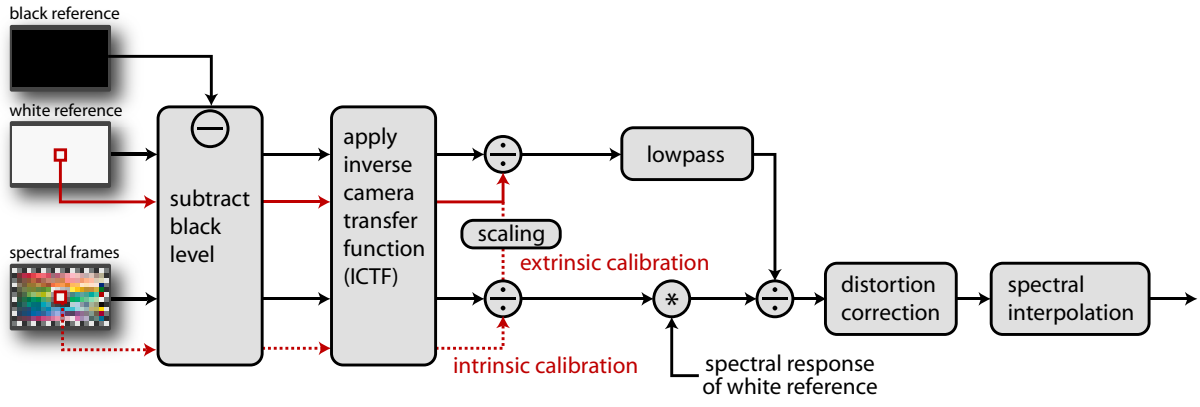

Figure 5: Processing pipeline.

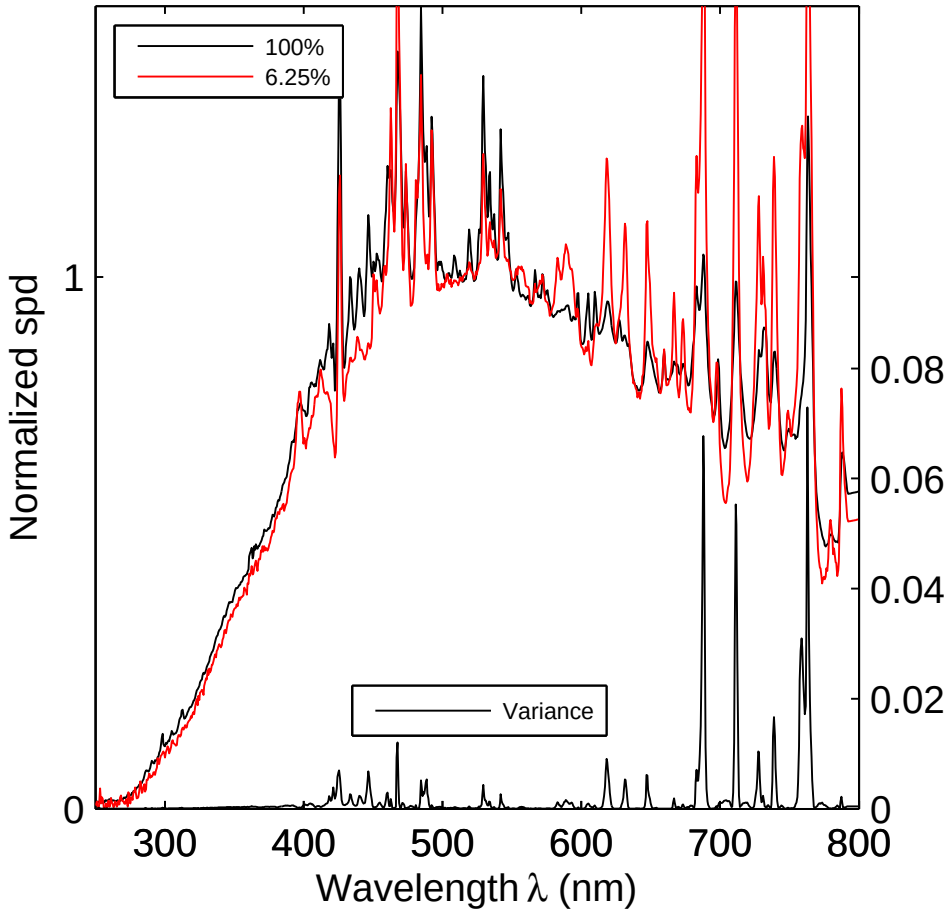

Figure 6: Normalized spectral power distribution (spd) of the flash for lowest and highest flash intensity (100% and 6.25%); the variance plot of the spectra (bottom of figure) takes five intensity settings into account.

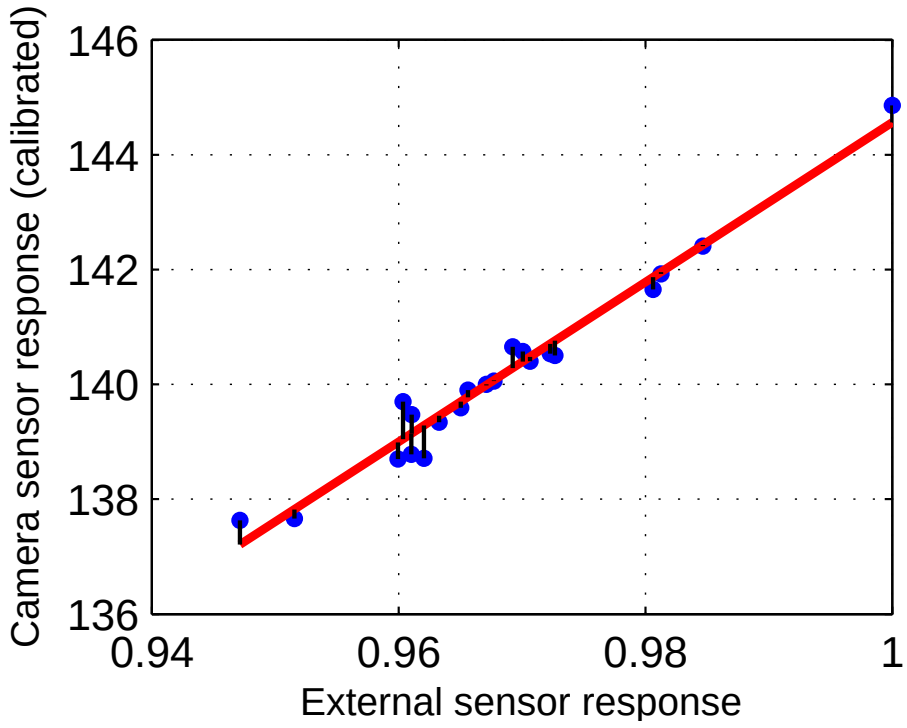

Figure 7: Simultaneous measurement of the flash intensity with an external sensor (transformed to luminance Y of the XYZ color space) and the camera.

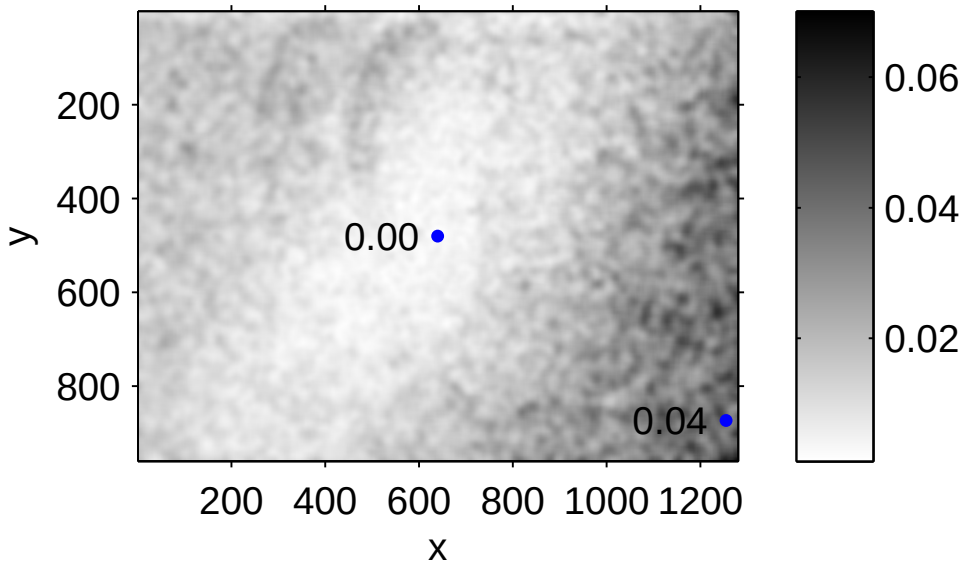

Figure 8: Temporal variation of illumination uniformity for our setup; values denote the variance of an 8 bit image stack.

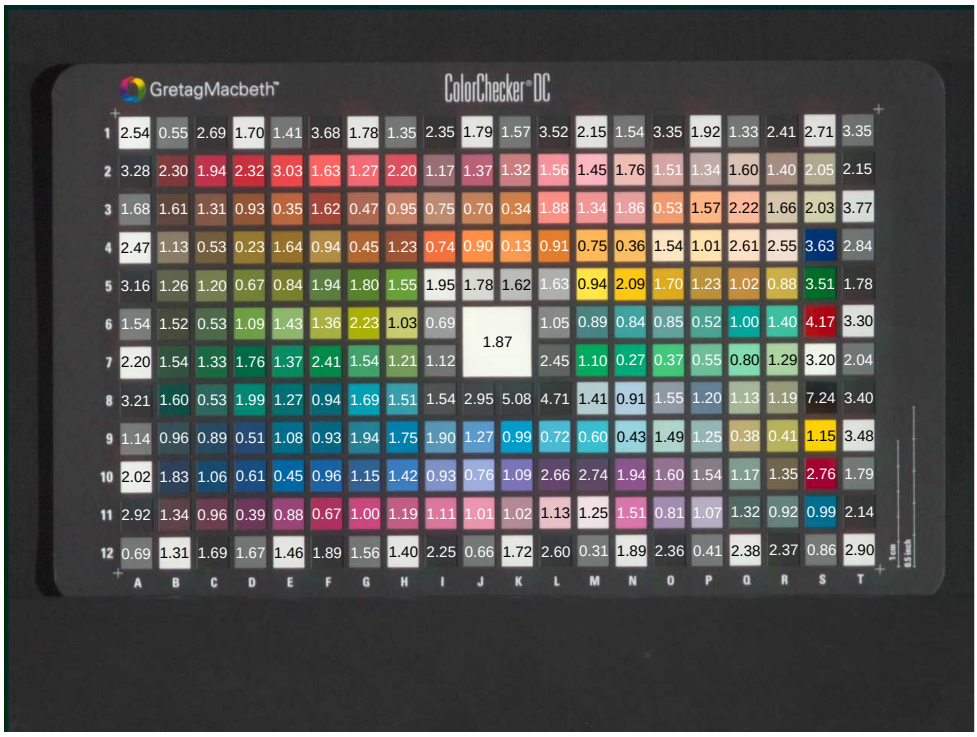

Figure 9: ColorChecker DC acquired with a flash light source and the corresponding ΔE_{00} errors.

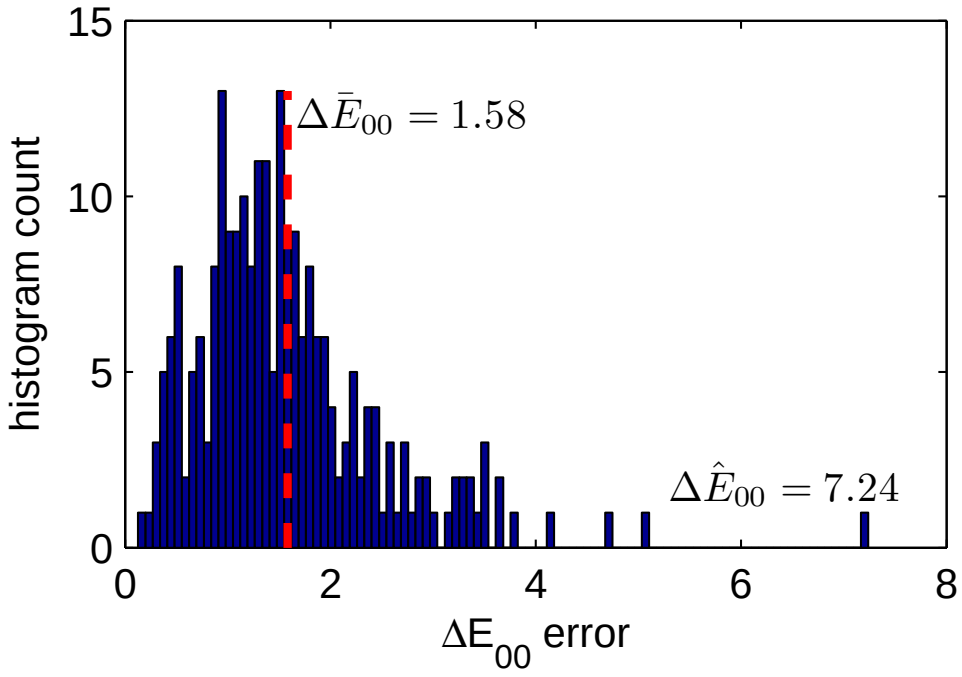

Figure 10: Histogram of ΔE_{00} errors depicted in Fig. 9.

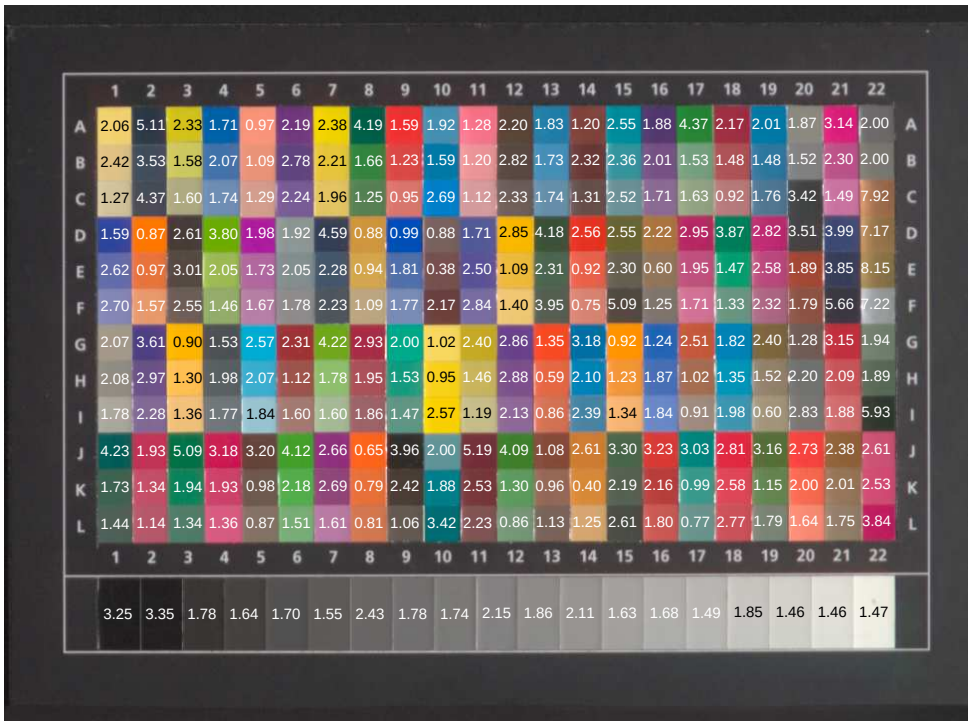

Figure 11: TE 221 test chart acquired with a flash light source and the corresponding ΔE_{00} errors.

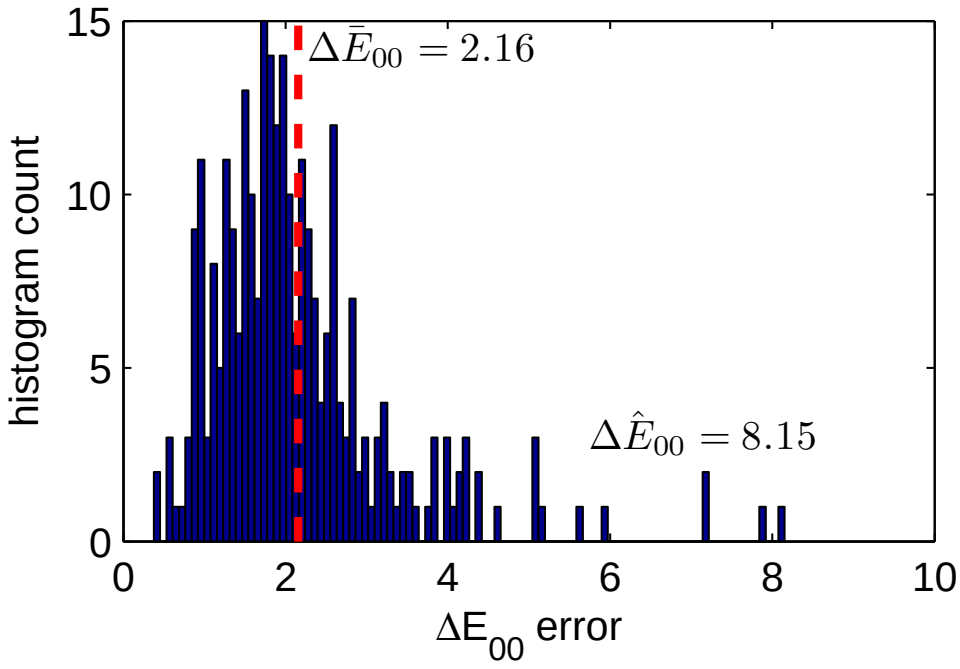

Figure 12: Histogram of ΔE_{00} errors depicted in Fig. 11.